La2-xPrxNiO4+δ as suitable cathodes for metal supported SOFCs

Vaibhav Vibhu, Aline Rougier, Clément Nicollet, Aurélien Flura, Jean-Claude Grenier, Jean-Marc. Bassat

$La_{2-x}Pr_xNiO_{4+\delta}$ as suitable cathodes for Metal Supported SOFCs

Vaibhav Vibhu, Aline Rougier, Clément Nicollet, Aurélien Flura, Jean-Claude Grenier and Jean-Marc Bassat*

CNRS, Université de Bordeaux, Institut de Chimie de la Matière Condensée de Bordeaux (ICMCB), 87 Av. Dr Schweitzer, F-33608 Pessac Cedex, France.

Abstract

Aiming at a tradeoff between the chemical stability of $La_2NiO_{4+\delta}$ (LNO) and the high electrochemical performances of $Pr_2NiO_{4+\delta}$ (PNO), $La_{2-x}Pr_xNiO_{4+\delta}$ mixed nickelates, further referred as LPNO, were studied as possible oxygen electrodes for Solid Oxide Fuel Cells (SOFCs). LPNO phases were synthesized using the modified citrate-nitrate route followed by a heat treatment at 1200 °C for 12h under air. Structural characterizations of those K_2NiF_4-type compounds show the existence of two solid solutions with orthorhombic structure, namely a La rich one from x = 0 to 0.5 with *Fmmm* space group, and a Pr rich one from x = 1.0 to 2.0 with *Bmab* space group. The mixed ionic and electronic conducting (MIEC) properties of LPNO phases were investigated through the evolution of the oxygen over-stoichiometry, δ, measured as a function of temperature and pO_2, the electrical conductivity, the diffusion and surface exchange coefficients versus x, showing that all compositions exhibit suitable characteristics as cathode materials for SOFCs. In particular, the electrochemical performances measured in symmetrical cells using LPNO materials sintered under low pO_2, as requested in Metal Supported Cell, (MSC-conditions) confirmed a decrease in polarization resistance values, R_p, from 0.93 Ω.cm² (LNO) down to 0.15 Ω.cm² (PNO) at 600 °C with increasing x.

Keywords: SOFCs, Metal Supported Cells, oxygen over-stoichiometry, lanthanum-praseodymium mixed nickelates, oxygen diffusivity

∗ Corresponding author at: CNRS, Université de Bordeaux, Institut de Chimie de la Matière Condensée de Bordeaux (ICMCB), 87 Av. Dr Schweitzer, F-33608 Pessac Cedex, France.
Tél.: +33 (0)5 40 00 27 53; Fax: +33 (0)5 40 00 27 61.
E-mail address: bassat@icmcb-bordeaux.cnrs.fr

1 Introduction

Solid Oxide Fuel Cells (SOFCs) are good candidates for clean energy technology converting hydrogen into electricity through a clean electro-chemical process. Indeed, fuel cells provide many advantages over traditional energy conversion systems including high efficiency, modularity and fuel adaptability [1, 2]. However, SOFCs are not used in large scale mainly because of issues related to the use of hydrogen, durability and also economic reasons. The challenging issues facing the development of economically competitive SOFCs include lowering the operating temperature from about 1000 ^{o}C down to 600 - 700 ^{o}C, in an intermediate temperature (IT) range so-called IT-SOFCs, in order to reduce their overall cost and increase their lifetime [3]. IT-SOFCs should reduce the thermal degradation and enable the use of low cost interconnect materials such as ferritic stainless steel.

Nowadays, metal supported cells (MSCs), also called 3rd generation of SOFC, are an attractive option for IT-SOFCs [4-11]. The main advantages of MSCs are summarized here, *i.e.* a) both electrode and electrolyte layers successively deposited on the metal support are thin, as a result the cost will be lower, b) an easier thermal cycling is anticipated, c) the metal support acts as a good current conductor due to its high electrical conductivity, d) the metal support is more ductile than the anode supported cells and e) MSCs can be used at intermediate operating temperatures. In most cases, a four-layer structure is commonly used for MSCs, consisting of thick porous alloy

substrates and three thin functional layers - a dense electrolyte in between porous anode and cathode.

The main issue for MSCs deals with the chemical stability of the components at high temperature and under low pO_2, which are the sintering conditions required to avoid any detrimental oxidation of the metal support as for instance using N_2 atmosphere ($pO_2 \approx 10^{-4}$ atm). In this study, the work is focused on the cathodic part. In this respect, new cathode materials with mixed ionic and electronic conducting (MIEC) properties at intermediate temperature have to be developed, exhibiting good chemical stability as well as high activity towards the electrochemical oxygen reduction reaction in the 600 - 700°C operating temperature range.

There are mainly two kinds of MIEC materials; the first one concerns oxygen deficient oxides, for example LSC ($La_{0.8}Sr_{0.2}CoO_{3-\delta}$), LSCF ($La_{0.4}Sr_{0.6}Co_{0.8}Fe_{0.2}O_{3-\delta}$) *etc*. The three main disadvantages of Sr-containing materials are a) their high values of thermal expansion coefficients (TECs) [12, 13], b) they react with zirconia to form $SrZrO_3$ insulating phase [14] and c) they easily form $SrSO_4$ insulating phase in presence of sulphur [15] , leading to a degradation of the cell performances.

Another type of MIEC oxides deals with oxygen over-stoichiometry, for example nickelates $Ln_2NiO_{4+\delta}$ (Ln = La, Pr, Nd) [16, 17]. These compounds with the K_2NiF_4 -type layered structure have shown promising cathode performances for IT-SOFCs because of their large anionic bulk diffusion as well as surface exchange coefficients, combined with good electrical conductivity and thermal expansion properties matching with those of yttria-stabilized zirconia (YSZ) or $Ce_{0.8}Gd_{0.2}O_{2-\delta}$ (GDC) used as electrolytes [18-21]. The structure of $Ln_2NiO_{4+\delta}$ consists of alternate NiO_2 square plane layers and Ln_2O_2 rock salt type-layers, leading to the first member (n=1) of the Ruddlesden-Popper series $Ln_{n+1}Ni_nO_{3n+1}$. This type of structure has a strong ability to accept

interstitial oxygen located in the Ln_2O_2 rock-salt interlayer leading to a mixed valence of Ni (Ni^{2+}/Ni^{3+}), which further results in a mixed ionic and electronic conductivity (O^{2-}/e^-) [18]. The δ-value (the amount of interstitial oxygen) is closely dependent on the rare-earth cation size. For instance, the oxygen excess in $La_2NiO_{4+\delta}$ (LNO) is $\delta \sim 0.16$ at room temperature, as reported by Zhao *et al.* [22]. On the opposite, $Pr_2NiO_{4+\delta}$ (PNO) shows a larger amount of interstitial oxygen ($\delta \approx 0.22$), resulting from the smaller ionic radius of Pr^{3+} ((r (Pr^{3+}) = 1.126 Å and r (La^{3+}) = 1.16 Å) [23] that induces large structural stresses released by a larger oxygen insertion [24, 25].

The polarization resistance (R_p) of the $Ln_2NiO_{4+\delta}$ (Ln = La, Pr, Nd) compounds deduced from electrochemical impedance spectroscopy measurements performed on symmetrical cells shows that the smallest values are obtained for the Pr phase [26], while LNO shows better chemical stability under low pO_2 [27].

The present work is focused on praseodymium substituted lanthanum nickelates $La_{2-x}Pr_xNiO_{4+\delta}$ ($0.0 \leq x \leq 2.0$). LPNO phases were synthesized and characterized in particular with respect to MSC conditions. In that respect the chemical stability as well as oxygen over-stoichiometry of the mixed nickelates were in a first part investigated under high temperature (1000 °C) and low pO_2 conditions (down to 10^{-4} atm).

The main goal of the work being to find an optimized composition with the required properties in order to be used as a cathode for metal supported cells, the conductivity as well electrochemical measurements were performed at high temperature in the operation conditions of the SOFC, *i.e.* under air.

2 Experimental

2.1 Chemical Synthesis and Characterization of the Powders

LPNO phases ($0.0 \leq x \leq 2.0$) were prepared using the citrate-nitrate route (modified Pechini method) [28] from Pr_6O_{11} (Aldrich chem, 99.9%), La_2O_3 (Strem Chemical, 99.99%) and $Ni(NO_3)_2{,}6H_2O$ (Acros Organics, 99%) precursors. Pr_6O_{11} and La_2O_3 were pre-fired in a first step at T = 900 °C overnight to remove the water content, due to their high hygroscopic character, then to weight the exact amount of precursors. The final annealing was performed at 1200 °C for 12 h in air, leading to well crystallized phases. The obtained powders were attrited with zirconia balls and ethanol for 4 h with the aim to obtain a mean particle size of about 0.6 µm (as checked using laser granulometry measurements).

The powders were characterized by X-Ray diffraction (XRD) at room temperature using a PANanalytical X'pert MPD diffractometer with Cu-K_α incident radiation.

Thermogravimetry analyses (TGA) were carried out using a TA Instrument TGA-Q50 device, with the aim i) to determine the delta values (at room temperature) of the various nickelates under air and ii) to study the δ variation *vs.* T under air as well as Ar atmospheres. In the first case the powders were previously heated under air up to 1000 °C then cooled down to room temperature with a slow rate (2 °C.min^{-1}), this cycle being reproduced twice to ensure the reproducibility. Then a second cycle was performed under Ar - 5% H_2 flux with a very slow heating rate of (0.5 °C.min^{-1}), the complete decomposition of the materials leading to determine the oxygen stoichiometry after cycling the sample down to room temperature [29]. Secondly, the variation of the oxygen stoichiometry of the materials was studied either under air (pO_2 = 0.21 atm) or Ar atmosphere (pO_2 $\approx 10^{-4}$ atm). For this purpose, the powders were first thermodynamically equilibrated under air in the TGA device as described above (*i.e.* two cycles were performed). Then the gas was changed from air to Ar at high temperature for faster solid/gas reactivity, and the same experiment was

performed under Ar. Both experiments show a reversible oxygen exchange, at least along the second thermal cycle, the TGA curves being perfectly reversible.

Thermal variations of the relative expansion of dense pellets (*dL/L*) were carried out in the temperature range 25 - 1000 °C, under air using a differential dilatometer (Netzsch® 402 ED), with the aim to determine the TECs of the materials.

The electrical conductivity of the materials was determined under air using the four-probe technique, in the temperature range 25 - 1000 °C with the heating and cooling rate of 1 °C.min^{-1}. The nickelates were previously sintered at 1350 °C for 4 h in order to get dense pellets.

The oxygen diffusion coefficient D^* and surface exchange coefficient k^* were determined by the so-called isotopic exchange depth profile (IEDP) technique combining isotopic exchange of ^{18}O (used as an oxygen tracer) for ^{16}O then secondary ion mass spectrometry (SIMS) analyses [30, 31]. The ceramics were first abraded with silicon carbide papers of successive grades, and then polished with an alumina paste down to a roughness close to 0.3 µm. The samples were annealed at a pressure of 210 mbar in an ^{18}O enriched atmosphere (97%, Eurisotop) for $500 < T\,°C < 700$. The ^{18}O penetration profiles, *i.e* normalized ^{18}O isotopic fraction (^{18}O / (^{16}O + ^{18}O)), were recorded as a function of the analyzed depth using a Cameca® IMS 6F SIMS apparatus with a Cs^+ ions source [32]. The oxygen profiles were then fitted usingan appropriate solution to the diffusion equation given by Crank, for a solution of the second Fick's law of gas diffusion in solids [33].

For the electrochemical studies, symmetrical half cells (electrode/GDC/8YSZ/GDC/electrode) were prepared. Dense pellets of 8YSZ (8 mol.% yttria stabilized zirconia) with diameter ≈ 18 mm and thickness ≈ 1.2 mm were used. Terpineol-based slurries were prepared for each nickelate or GDC powder (from Rhodia). In order to increase the electrochemical performances of the half-

cells [26], a 2µm GDC layer was initially screen printed on both sides of the 8YSZ electrolyte pellet and sintered at 1300 °C for 1 h under air. The nickelate layer (thickness ≈ 20 µm) was then screen printed on each side. The optimal sintering temperature of the cathode previously determined in air was 1150 °C for 1 h [26]. A similar study was performed for sintering conditions under low pO_2 (≈ 10^{-4} atm.). Among three sintering temperatures T_s = 1100, 1150 and 1200 °C, the best electrochemical performance (i.e. lowest R_p value) was found at T_s = 1150 °C. Hence herein, sintering was performed at 1150 °C for 1 h under nitrogen ($pO_2 \approx 10^{-4}$ atm) [27]. The half-cells were re-oxidized at 800°C under air for 12 h before the measurements.

The electrochemical measurements were performed under air, using a two electrodes configuration with signal amplitude of 50 mV under zero current condition with the aim to determine the R_p values. The frequency range was scanned from 10^6 Hz to 10^{-2} Hz with 91 points, using an Autolab PGSTAT 302N, equipped with a frequency response analyzer (FRA). All the impedance diagrams were fitted using the Z-view® (Scribner Associates) software.

3 Results and Discussion

3.1 XRD characterizations

The XRD study shows that all LPNO phases with $0.0 \leq x < 0.5$ and $1.0 < x \leq 2.0$ are single phases, their patterns being indexed with an orthorhombic cell described either by the *Fmmm* space group for La rich solid solution [$0.0 \leq x < 0.5$] or *Bmab* space group for Pr rich solid solution [$1.0 < x \leq 2.0$]. Furthermore, full pattern matching was carried out using the FULLPROF software. As examples, for $La_{1.75}Pr_{0.25}NiO_{4+\delta}$ and $La_{0.5}Pr_{1.5}NiO_{4+\delta}$, a good agreement is obtained between the experimental and refined patterns (Fig. 1).

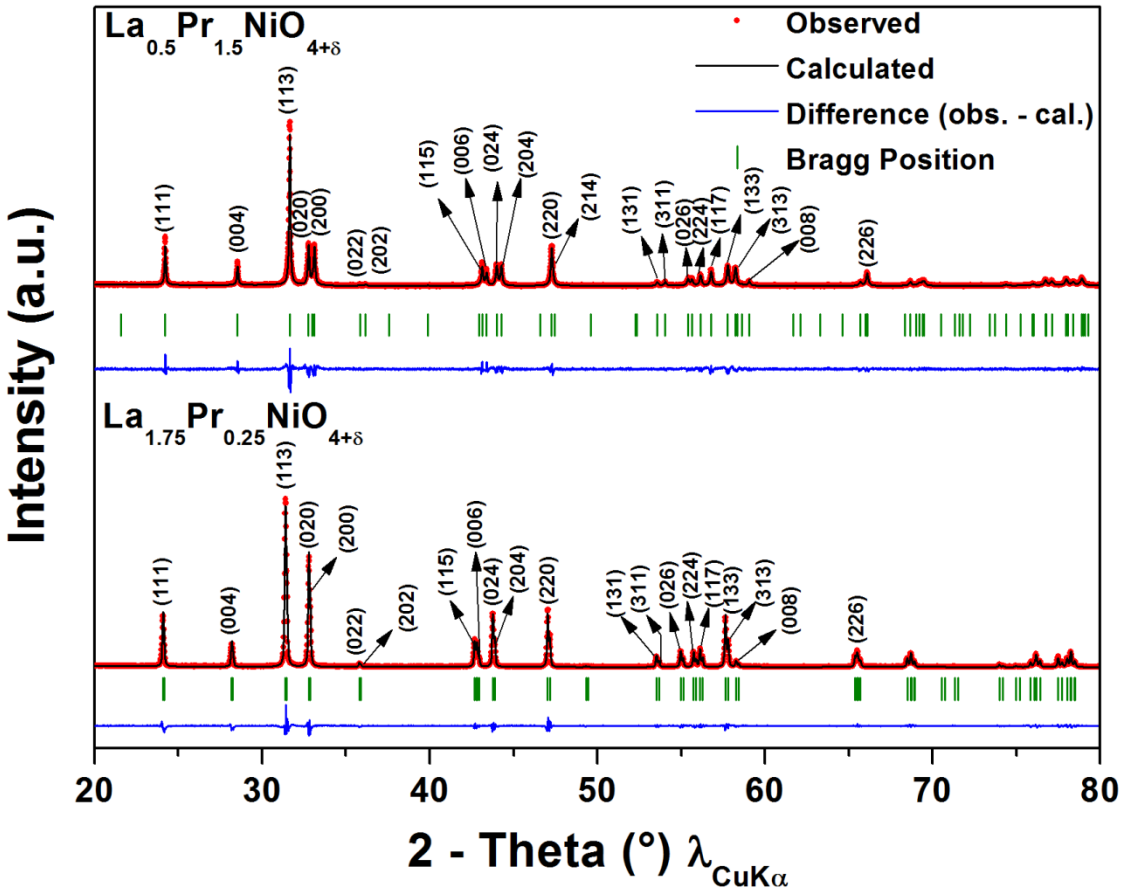

Fig. 1. Fullprof refinement of the X-ray patterns of $La_{1.75}Pr_{0.25}NiO_{4+\delta}$ and $La_{0.5}Pr_{1.5}NiO_{4+\delta}$ using Fmmm and Bmab space group, respectively. (2-column fitting image, color on the web)

For the XRD refinements, Bmab and Fmmm space groups were used for Pr and La-rich phases, respectively. The variation of the lattice parameters as a function of *x* is reported in Fig. 2. The substitution of lanthanum by praseodymium leads to a smooth decrease in each lattice parameters for both La rich and Pr-rich solid solutions. This decrease in *a* and *b* cell parameters with the increasing Pr content is consistent with the variation of the ionic radius [23] leading to an overall decrease in the cell volume. For the $x \approx 0.5$ - 1.0 region, the *a* parameter suddenly decreases while *b* suddenly increases suggesting a phase transition in agreement with the results reported by Allançon *et al.* [34] and Nishimoto *et al.* [35].

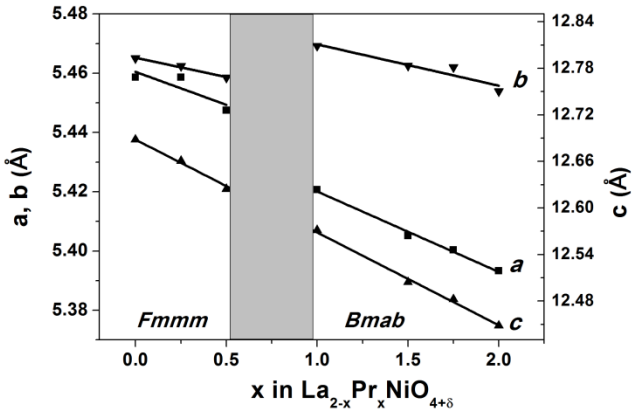

Fig. 2. Variation of the lattice parameters as a function of x for $La_{2-x}Pr_xNiO_{4+\delta}$. Grey region represents the biphasic region. (Single column fitting image)

The exact chemical composition corresponding to this phase transition is still to be determined. For this purpose, additional compositions (x = 0.6, 0.7, 0.75, 0.8 and 0.85) were synthesized and characterized. XRD patterns of those additional compositions could not be accurately fitted using a single space group, but was possible using simultaneously both *Fmmm* and *Bmab* space groups, which suggests the coexistence of two phases (biphasic region) in between x = 0.5 and x = 1.0, represented by grey region in Fig.2Aiming at deeper understanding, synchrotron experiments are currently in progress.

3.2 Thermogravimetry analyses

The oxygen over-stoichiometry (δ) at room temperature for PLNO phases was calculated using the results of TGA experiments performed under reducing conditions (5% H_2/Ar atmosphere, heating rate 0.5 °C.min^{-1}). As earlier reported [29], two weight losses occur. The first one, around 400 °C, corresponds to the reduction of Ni^{3+} into Ni^{2+} (the oxygen over-stoichiometry being reduced down to δ = 0 when expecting only La^{3+} and Pr^{3+} cations). The second weight loss

characterizes the complete reduction of LPNO in appropriate ratio (*i.e. x* dependent) into La_2O_3, Pr_2O_3 and Ni, leading to the determination of $1+\delta$. The value of δ was also calculated *via* iodometric titration of the Ni^{2+}/Ni^{3+} couple [18]. The δ values calculated by iodometry and TGA are gathered in Table 1. As expected, an increase of δ, from 0.16 (LNO) to 0.25 (PNO), is evidenced with praseodymium substituting lanthanum. In this study, the δ value for PNO (δ = 0.25) is slightly higher than that earlier reported (δ = 0.22) [25]. This is probably due to small differences in the Pr over Ni ratio, which can easily decrease at least down to 1.95 leading to a simultaneous decrease in δ, as evidenced in previous works for LNO [20, 36]. In the present work the Pr/Ni ratio is equal to 2 as determined by ICP measurements, probably explaining the higher δ value.

Table 1 Oxygen over-stoichiometry δ calculated from TGA and iodometry measurements, and the average δ value.

Nickelates	**δ (by TGA)**	**δ (by Iodometry)**	**δ (average)**
$La_2NiO_{4+\delta}$	0.16	0.16	0.16
$Pr_{0.5}La_{1.5}NiO_{4+\delta}$	0.16	0.17	0.17
$PrLaNiO_{4+\delta}$	0.19	0.19	0.19
$Pr_{1.5}La_{0.5}NiO_{4+\delta}$	0.22	0.20	0.21
$Pr_2NiO_{4+\delta}$	0.25	0.25	0.25

The thermal variations of the oxygen content, $4+\delta$, under air for the $La_{2-x}Pr_xNiO_{4+\delta}$ phases and under air and Ar (*i.e.*, $pO_2 = 2.10^{-4}$ atm) for $LaPrNiO_{4+\delta}$ are plotted in Fig. 3 and Fig. 4, respectively. The result obtained for $La_2NiO_{4+\delta}$ is in agreement with Nakamura et al. [37].

(a)

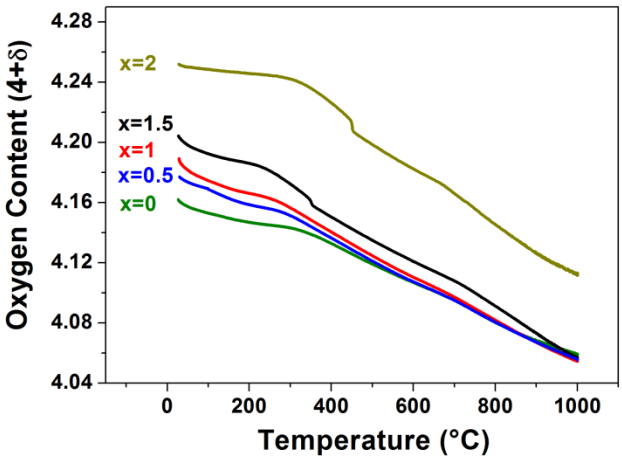

(b)

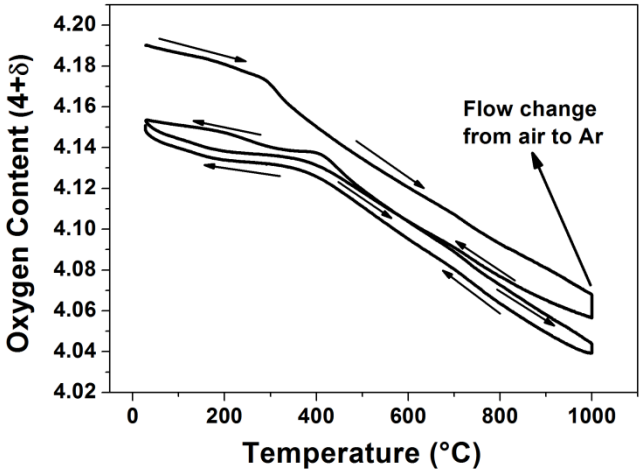

Fig. 3. Thermal variation of the oxygen content ($4+\delta$) (30 °C $\leq T \leq$ 1000 °C) for $La_{2-x}Pr_xNiO_{4+\delta}$, under air and for $LaPrNiO_{4+\delta}$ under air and Ar. (Single column fitting image, color on the web).

All LPNO nickelates remain always oxygen over-stoichiometric within the whole temperature range under air and Ar atmosphere. This behavior indicates that all these materials always exhibit MIEC properties under air and under low pO_2 conditions. A sudden uptake of oxygen around $T \approx$

400 °C is evidenced under air upon cooling for PNO (x = 2) and for $La_{0.5}Pr_{1.5}NiO_{4+\delta}$ (x = 1.5) (Fig. 3). Current investigations in our group show that this transition is related to structural changes [38]. The small drop in oxygen content ($\Delta\delta$ = 0.02) after changing the gas flow from air to Ar (Fig. 4) results from the loss of oxygen under low pO_2 condition.

3.3 Electrical Conductivity Measurements

The variation of the total electrical conductivity σ *vs.* 1000/T under air for LPNO compounds is reported in Fig. 4.

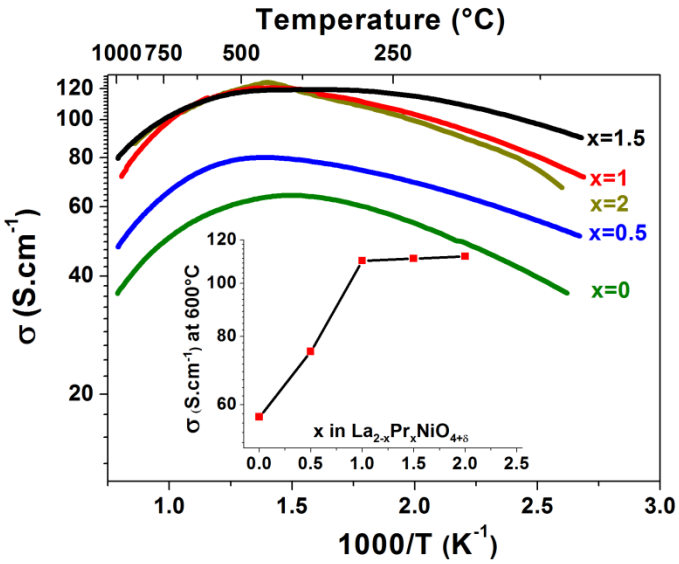

Fig. 4. Thermal variation of the electrical conductivity measured under air for $La_{2-x}Pr_xNiO_{4+\delta}$. (Single column fitting image, color on the web)

The nickelates exhibit a semi-conducting behavior for T < 600 °C, with a maximum of conductivity observed in the 400-600 °C range. Above this temperature range, their conductivity decreases; this

pseudo-metallic behavior is directly correlated to the decrease of oxygen content as evidenced by TGA data (Fig. 3) and correspondingly to the decrease of the hole carrier density even though the compounds remain semi-conducting [20]. Pr-containing phases exhibit higher conductivity than LNO in the considered temperature range. As an example, a small addition of Pr in LNO (x = 0.5) leads to an increase of the conductivity from 50 to 70 $S.cm^{-1}$ at 600 °C. For x = 1, 1.5 or 2, (*i.e.* high praseodymium contents), the conductivity largely increases, being about twice the one of LNO, reaching a value close to 110 $S.cm^{-1}$ at 600 °C for the three compositions (inset in Fig. 4). Praseodymium-rich compositions are then of high interest to determine the best compromise, at least regarding the conductivity values at the operating temperature.

3.4 Dilatometry Measurements

The thermal variations of the relative expansion dL/L measured under air for LPNO phases are reported in Fig. 5. The thermal expansion coefficients (TECs), calculated from the slope of the corresponding straight lines in the full range of temperature are in between 13 to 13.5 × 10^{-6} $°C^{-1}$ for all nickelates, indicating that from a thermo-mechanical point of view these nickelates can be used in SOFCs involving 8YSZ as well as GDC as electrolytes [38]. It should be useful to consider the part of the so-called chemical expansion which is normally included in the whole thermal expansion here measured. Indeed, because the changes in temperature as well as oxygen partial pressure often result, at least for for simple oxides, in changes on the starting (at room temperature) oxygen stoichiometry, as described for instance by Bishop, an expansion due to reduction of multivalent cations combined to a contraction due to relaxation of ions around oxygen vacancies would appear [VV please include ref Bishop 2013]. However, in MIEC materials with perovskite structured oxides such as nickelates here studied, the origin of the chemical expansion is less well

understood. Moreover, because no major deviation is experimentally observed in the dL/L *vs.* T curve at high temperature, the chemical expansion part of the TEC has not been discussed here.

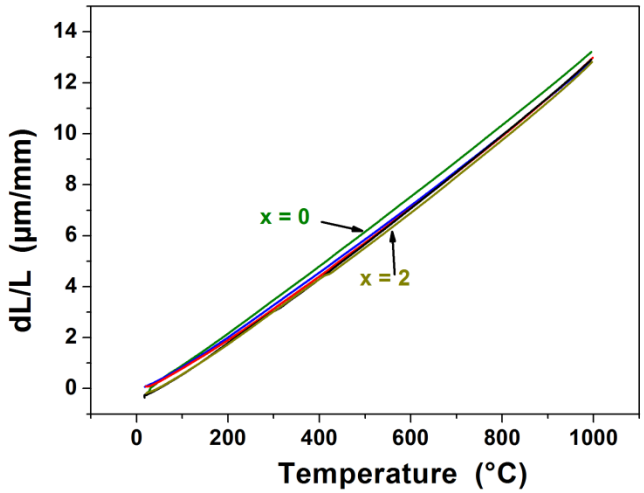

Fig. 5. Thermal variation of the relative expansion (dL/L) for $La_{2-x}Pr_xNiO_{4+\delta}$, under air (30 °C ≤ T ≤ 1000 °C). (Single column fitting image, color on the web)

3.5 Oxygen diffusion and surface exchange coefficients (D, k*)*

The thermal variation of the oxygen diffusion coefficients, D^*, and surface exchange coefficients, k^*, for LPNO (x = 0.5, 1 and 1.5) are plotted in Figure 7, for T = 500, 600, 650 and 700 °C. At first, the D^* values are comparable to those reported for PNO (3×10^{-8} $cm^2.s^{-1}$) and LNO (1.5×10^{-8} $cm^2.s^{-1}$) at 600 °C [18]. It is worth mentioning that these values are among the highest ones available in the literature, especially at low temperatures (around 500 < T °C < 600) due to a low activation energy (0.6 to 0.7 eV, against 1.4 to 1.8 eV for the perovskite-type materials) [32]. As an example the D* plots *vs.* T for LSCF material is given on fig. 6a.

(a)

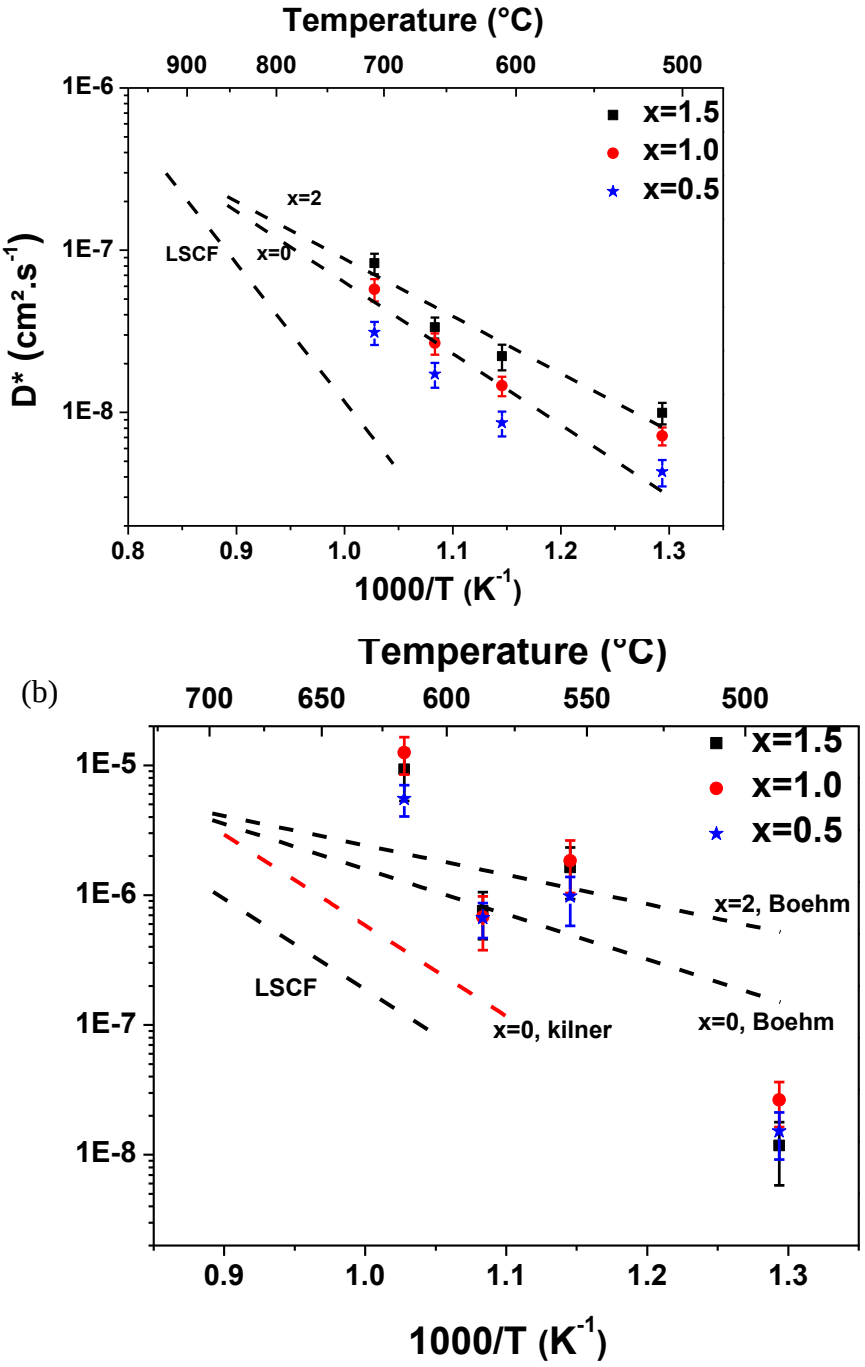

Fig. 6. Thermal variation of (a) the diffusion coefficient *D** and (b) the surface exchange coefficient *k** for $La_{2-x}Pr_xNiO_{4+\delta}$ (x = 0.5, 1 and 1.5). The plotted error bars represent the deviation

from the average value of the coefficients determined using three different analysis in each case. (Single column fitting image, color on the web)

The D^* values for all LPNO phases are close to each other (Fig. 6(a)) whatever the temperature, while remaining higher for the Pr rich solid solution. The diffusion coefficients of mixed nickelates are intermediate between earlier reported LNO and PNO ceramics. The value increases with increasing Pr-content. Once again, because the diffusion coefficients in the whole solid solution are found in between less than an order of magnitude at a given temperature, the ionic conductivity would normally not be a penalizing parameter, whatever the mixed nickelates composition, with respect to the SOFCs application.

Regarding the k^* values (Fig. 6(b)), they are slightly higher at high temperature than those reported for PNO and LNO [18]. However, the k^* values highly depend on the surface state of the ceramics, itself being dependent on the grain size for similar polishing conditions. In addition, at a given temperature, the various k^* values are found in a range less than one order of magnitude.

3.6 Electrochemical Measurements

The impedance diagrams were recorded in the temperature range 500-800 °C under air following the sintering of the electrodes at high temperature under low pO_2 as detailed in the experimental part, then allowing the determination of R_p. The R_p values were obtained by fitting the impedance diagrams recorded for all the LPNO half cells with two $R\|CPE$ (constant phase element) in series, which is the simplest equivalent circuit model that yields a good fit to the data. However, the EIS diagram of the LNO electrode was fitted using Gerischer impedance as reported in earlier studies [39, 40]. In the current study the fit was limited to the extraction of the R_p value, therefore no attempt was made to interpret the two elements representing the total electrode processes.

The Nyquist impedance diagrams for LPNO electrodes, at 600 °C, are shown in Fig. 7 (a), whereas Fig. 7 (b) represents a typical fit of impedance data for the $La_{1.5}Pr_{0.5}NiO_{4+\delta}$ electrode (600 °C) using two *R*‖*CPE* elements.

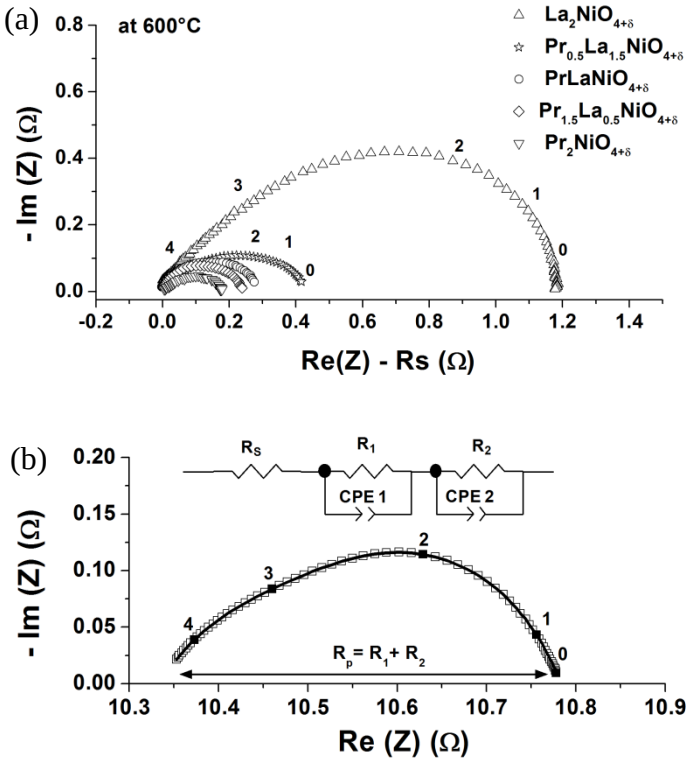

Fig. 7. (a) Nyquist plots recorded for LPNO electrodes at 600 °C, (b) Impedance diagram for $La_{1.5}Pr_{0.5}NiO_{4+\delta}$ in symmetrical half cell at 600 °C, fitted using R_s (series resistance), R_1‖CPE_1 and R_2‖CPE_2. (Single column fitting image)

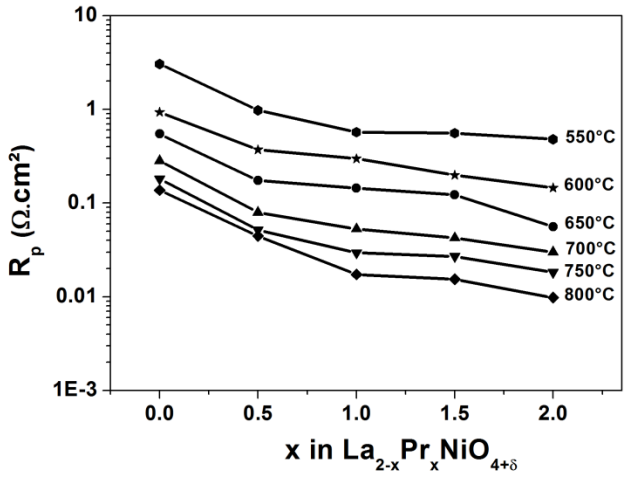

Fig. 8. Composition dependence of the polarization resistance, R_p, for $La_{2-x}Pr_xNiO_{4+\delta}$ phases in the 550 °C to 800 °C temperature range. (Single column fitting image)

The variations of calculated R_p for LPNO electrodes, in the 550 °C to 800 °C temperature range, as a function of x are shown in Fig. 8. The electrochemical performance is notably improved (i.e. decrease of R_p) by the substitution of La by Pr, whatever the temperature. For instance, a R_p value of 0.93 Ω.cm² is achieved at 600 °C for LNO while after substitution of La by Pr, the R_p values decrease down to 0.37, 0.29, 0.23 and 0.15 Ω.cm² for $La_{1.5}Pr_{0.5}NiO_{4+\delta}$, $LaPrNiO_{4+\delta}$, $La_{0.5}Pr_{1.5}NiO_{4+\delta}$ and PNO, respectively (Fig. 8). Whatever the temperature, R_p notably decreases nonlinearly with increasing Pr content, for example, by 3 times (0.93 to 0.37 Ω.cm²) from LNO to $La_{1.5}Pr_{0.5}NiO_{4+\delta}$. From those preliminary results, it can be concluded that the best electrochemical properties (*i.e.* lowest R_p) are achieved with the PNO electrode. However, as mentioned in the introduction, a definite conclusion requires the study of long term ageing experiments. For this purpose, the chemical stability of the LPNO nickelates under air at operating temperatures as well as the variation of R_p during ageing

(recorded under air at i_{dc} = 0 and $i_{dc} \neq 0$ conditions) are currently under investigation for duration up to one month. LNO is highly stable whereas PNO is completely dissociated after 1 month at 600, 700 and 800°C. Interestingly, the ageing of the mixed LPNO/CGO/8YSZ half cells during 1 month under air shows no change in the R_p value at i_{dc} = 0 condition. The complete and detailed description of these experiments will be reported in a forthcoming paper.

4 Conclusions

The present study is focused on alternative oxygen electrodes for IT-SOFCs prepared in MSC-type conditions, *i.e.* under low pO_2. Belonging to the K_2NiF_4 structural type, the $La_{2-x}Pr_xNiO_{4+\delta}$ mixed nickelates (LPNO) were synthesized and depending on the La/Pr ratio, two domains of solid solutions with orthorhombic structure were identified. One is related to La-rich phases, from x = 0 to x = 0.5, with the *Fmmm* space group while Pr-rich phases, from x = 1.0 to x = 2, crystallize with *Bmab* space group. All the Lanthanum-Praseodymium nickelates are oxygen over-stoichiometric in the whole temperature range either under air or argon. The δ value increases with increasing x. All other physico-chemical properties including electrical conductivity, TECs, oxygen diffusion and surface exchange coefficients confirm the suitability of LPNO for MS-SOFCs application. Besides, the decrease in the polarization resistance as a function of x suggests that the Pr-rich compounds are more efficient for the oxygen electrode reaction than the La-rich ones. Studies of ageing behavior especially at the operating conditions are in progress.

Acknowledgement

This work was performed under PEREN project (reference: ANR-2011-PREG-016-05). The authors wish to gratefully acknowledge the Agence Nationale de la Recherche (A.N.R., France) for supporting these scientific works and for the financial support. Authors also acknowledge to Eric Lebraud for XRD, Nicolas Penin and Sébastien Fourcade for their valuable helps in the experiments.

References

[1] E. Ivers-Tiffée, A. Weber, D. Herbstritt, Materials and Technologies for SOFC-components, Journal of the European Ceramic Society 21 (2001) 1805–1811.

[2] A. J. Jacobson, Materials for Solid Oxide Fuel Cells, Chemistry of Materials 22 (3) (2010) 660–674.

[3] D. J. L. Brett, A. Atkinson, N. P. Brandon, S. J. Skinner, Intermediate Temperature Solid Oxide Fuel Cells, Chemical Society Reviews 37 (8) (2008) 1568–1578.

[4] I. Villarreal, C. Jacobson, A. Leming, Y. Matus, S. Visco, L. De Jonghe, Metal-Supported Solid Oxide Fuel Cells, Electrochemical and Solid-State Letters 6 (9) (2003) A178–A179.

[5] Y. B. Matus, L. C. De Jonghe, C. P. Jacobson, S. J. Visco, Metal-Supported Solid Oxide Fuel Cell membranes for rapid thermal cycling, Solid State Ionics 176 (2005) 443–449.

[6] S. Hui, D. Yang, Z. Wang, S. Yick, C. Decès-Petit, W. Qu, A. Tuck, R. Maric, D. Ghosh, Metal-Supported Solid Oxide Fuel Cell operated at 400-600 °C, Journal of Power Sources 167 (2) (2007) 336–339.

[7] M. C. Tucker, G. Y. Lau, C. P. Jacobson, L. C. DeJonghe, S. J. Visco, Performance of Metal-Supported SOFCs with infiltrated electrodes, Journal of Power Sources 171 (2) (2007) 477–482.

[8] M. C. Tucker, G. Y. Lau, C. P. Jacobson, L. C. DeJonghe, S. J. Visco, Stability and robustness of Metal-Supported SOFCs, Journal of Power Sources 175 (1) (2008) 447–451.

[9] S. Sakuno, S. Takahashi, H. Sasatsu, Metal-Supported SOFC development at JPOWER, ECS Transaction 25 (2) (2009) 731–737.

[10] M. C. Tucker, Progress in Metal-Supported Solid Oxide Fuel Cells: A review, Journal of Power Sources 195 (15) (2010) 4570–4582.

[11] Y. Zhou, X. Xin, J. Li, X. Ye, C. Xia, S. Wang, Z. Zhan, Performance and degradation of Metal-Supported Solid Oxide Fuel Cells with impregnated electrodes, International Journal of Hydrogen Energy 39 (5) (2014) 2279–2285.

[12] G. Ch. Kostogloudis, Ch. Ftikos, Properties of A-site-deficient $La_{0.6}Sr_{0.4}Co_{0.2}Fe_{0.8}O_{3-\delta}$-based perovskite oxides, Solid State Ionics 126 (1) (1999) 143–151.

[13] V. V. Kharton, A. P. Viskup, D. M. Bochkov, E. N. Naumovich, O. P. Reut, Mixed electronic and ionic conductivity of $LaCo(M)O_3$ (M = Ga, Cr, Fe or Ni) III. Diffusion of oxygen through $LaCo_{1-x-y}Fe_xNi_yO_{3\pm\delta}$ ceramics, Solid State Ionics 110 (1998) 61–68.

[14] G. Ch. Kostogloudis, G. Tsiniarakis, Ch. Ftikos, Chemical reactivity of perovskite oxide SOFC cathodes and yttria stabilized zirconia, Solid State Ionics 135 (2000) 529–535.

[15] F. Wang, K. Yamaji, D.-H. Cho, T. Shimonosono, H. Kishimoto, M. E. Brito, T. Horita, H. Yokokawa, Effect of Strontium concentration on Sulfur poisoning of LSCF cathodes, Solid State Ionics 225 (2012) 157–160.

[16] G. Amow, I. J. Davidson, S. J. Skinner, A comparative study of the Ruddlesden-Popper series, $La_{n+1}Ni_nO_{3n+1}$ (n = 1, 2 and 3), for Solid Oxide Fuel Cell cathode applications, Solid State Ionics 177 (2006) 1205–1210.

[17] S. Takahashi, S. Nishimoto, M. Matsuda, M. Miyake, Electrode properties of the Ruddlesden-Popper series, $La_{n+1}Ni_nO_{3n+1}$ (n = 1, 2, and 3), as Intermediate-Temperature Solid Oxide Fuel Cells, Journal of the American Ceramic Society 93 (8) (2010) 2329–2333.

[18] E. Boehm, J.-M. Bassat, P. Dordor, F. Mauvy, J.-C. Grenier, P. Stevens, Oxygen diffusion and transport properties in non-stoichiometric $Ln_{2-x}NiO_{4+\delta}$ oxides, Solid State Ionics 176 (2005) 2717–2725.

[19] A. Aguadero, J. A. Alonso, M. J. Martinez-Lope, M. T. Fernandez-Diaz, M. J. Escudero, L. Daza, In situ high temperature neutron powder diffraction study of oxygen-rich $La_2NiO_{4+\delta}$ in air: Correlation with the electrical behaviour, Journal of Materials Chemistry 16 (33) (2006) 3402–3408.

[20] J.-M. Bassat, P. Odier, J. P. Loup, The Semiconductor-to-metal Transition in question in $La_{2-x}NiO_{4+\delta}$, Journal of Solid State Chemistry 110 (1) (1994) 124–135.

[21] C. N. Munnings, S. J. Skinner, G. Amow, P. S. Whitfield, I. J. Davidson, Oxygen transport in the $La_2Ni_{1-x}Co_xO_{4+\delta}$ system, Solid State Ionics 176 (2005) 1895–1901.

[22] H. Zhao, F. Mauvy, C. Lalanne, J.-M. Bassat, S. Fourcade, J.-C. Grenier, New cathode materials for ITSOFC: Phase stability, oxygen exchange and cathode properties of $La_{2-x}NiO_{4+\delta}$, Solid State Ionics 179 (2008) 2000–2005.

[23] R. D. Shannon, Revised Effective Ionic Radii and Systematic Studies of Interatomic distances in Halides and Chaleogenides, Acta Crystallogr. Sect. A32 (1976) 751.

[24] D. J. Buttrey, P. Ganguly, J. M. Honig, C. N. R. Rao, R. R. Schartman, G. N. Subbanna, Oxygen Excess in Layered Lanthanide Nickelates, Journal of Solid State Chemistry 74 (2) (1988) 233–238.

[25] C. Allançon, A. Gonthier-Vassal, J.-M. Bassat, J. P. Loup, P. Odier, Influence of oxygen on structural transitions in $Pr_2NiO_{4+\delta}$, Solid State Ionics 74 (1994) 239–248.

[26] C. Ferchaud, J.-C. Grenier, Y. Zhang-Steenwinkel, M. M. A.Van Tuel, F. P. F. Van Berkel, J.-M. Bassat, High performance praseodymium nickelate oxide cathode for low temperature Solid Oxide Fuel Cell, Journal of Power Sources 196 (4) (2011) 1872–1879.

[27] A. Flura, S. Dru, C. Nicollet, S. Fourcade, A. Rougier, J.-M. Bassat, J.-C. Grenier, A. Brevet, J. Mougin, Chemical stability of $Ln_2NiO_{4+\delta}$ (Ln = La, Pr or Nd) under low pO_2 for cathodes in MSC-type devices, 5th International Conference on Fundamentals and Development of Fuel Cells, FDFC 2013 (2013).

[28] P. Courty, H. Ajot, C. Marcilly, B. Delmon, Oxydes Mixtes ou en Solution Solide sous forme Très Divisée Obtenus par Décomposition Thermique de Précurseurs Amorphes, Powder Technology 7 (1) (1973) 21–38.

[29] J. A. Kilner, C. K. M. Shaw, Mass transport in $La_2Ni_{1-x}Co_xO_{4+\delta}$ oxides with the K_2NiF_4 structure, Solid State Ionics 154-155 (2002) 523–527.

[30] R. A. De Souza, J. Zehnpfenning, M. Martin, J. Maier, Determining oxygen isotope profiles in oxides with Time-of-Flight SIMS, Solid State Ionics 176 (2005) 1465–1471.

[31] J.-M. Bassat, M. Petitjean, J. Fouletier, C. Lalanne, G. Caboche, F. Mauvy, J.-C. Grenier, Oxygen isotopic exchange: A useful tool for characterizing oxygen conducting oxides, Applied Catalysis A: General 289 (1) (2005) 84–89.

[32] E. Boehm, J.-M. Bassat, M. C. Steil, P. Dordor, F. Mauvy, J.-C. Grenier, Oxygen transport properties of $La_2Ni_{1-x}Cu_xO_{4+\delta}$ mixed conducting oxides, Solid State Sciences 5 (7) (2003) 973–981.

[33] J. Crank, The Mathematics of Diffusion, Clarendon Press, Oxford, 2nd Edition, 1975.

[34] C. Allançon, P. Odier, J.-M. Bassat, J. P. Loup, La and Sr Substituted $Pr_2NiO_{4+\delta}$: Oxygenation and Electrical Properties, Journal of Solid State Chemistry 131 (1) (1997) 167–172.

[35] S. Nishimoto, S. Takahashi, Y. Kameshima, M. Matsuda, M. Miyake, Properties of $La_{2-x}Pr_xNiO_{4+\delta}$ cathode for Intermediate-Temperature Solid Oxide Fuel Cells, Journal of the Ceramic Society of Japan 119 (3) (2011) 246–250.

[36] P. Odier, J.-M. Bassat, J. C. Rifflet and J. P. Loup, On thermo-Physical Poperties of $La_{2-x}NiO_{4+\delta}$, $\delta \geq 0$ or < 0, Solid State Communications 85 (7) (1993) 561-564.

[37] T. Nakamura, Y. Takeyama, S. Watanabe, K. Yashiro, K. Sato, T. Hashida, J. Mizusaki, Oxygen nonstoichiometry, Crystal structure and Mechanical properties of $Ln_2NiO_{4+\delta}$, 25 (2009) 2573–2580.

[38] A. Flura, C. Nicollet, V. Vibhu, S. Fourcade, E. Lebraud, A. Rougier, J.-M. Bassat, J.-C. Grenier, Chemical and structural changes of $Ln_2NiO_{4+\delta}$ (Ln = La, Pr or Nd) Lanthanide Nickelates as a function of oxygen partial pressure at high temperature, submitted to Journal of Solid State Chemistry.

[39] N. Hildenbrand, P. Nammensma, D. H. A. Blank, H. J. M. Bouwmeester, B. A. Boukamp, Influence of configuration and microstructure on performance of $La_2NiO_{4+\delta}$ Intermediate-Temperature Solid Oxide Fuel Cells cathodes, Journal of Power Sources 238 (2013) 442–453.

[40] G. T. Kim, A. J. Jacobson, Electrochemical Characterization of $La_{2-x}Pr_xNiO_{4+\delta}$ for Application as Cathodes in Intermediate Temperature SOFCs, Mater. Res. Soc. Symp. Proc. 972 (2007) 175–180.